Journal of Oceanology and Limnology

https://doi.org/10.1007/s00343-025-4208-z

Research Paper

Nutrient-mediated changes in growth, biochemical composition, and biosilica deposition in *Cyclotella cryptica**

Yuting YU[1], Yan SUN[1], Yuhang LI[2], Zhengfeng ZHU[1], Lin ZHANG[3], Jian LI[4], Spiros N. AGATHOS[5, 6], Chengxu ZHOU[1], Jichang HAN[1, **]

[1] *College of Food Science and Engineering, Ningbo University, Ningbo 315832, China*

[2] *Laboratory of Marine Organism Taxonomy and Phylogeny, Institute of Oceanology, Chinese Academy of Sciences, Qingdao 266071, China*

[3] *Key Laboratory of Applied Marine Biotechnology, Ministry of Education of China, Ningbo University, Ningbo 315832, China*

[4] *School of Biological and Chemical Engineering, Panzhihua University, Panzhihua 617000, China*

[5] *Earth & Life Institute, Bioengineering Laboratory, Catholic University of Louvain, Louvain-La-Neuve 1348, Belgium*

[6] *Qingdao Innovation and Development Base, Harbin Engineering University, Qingdao 266000, China*

Received Aug. 3, 2024; accepted in principle Oct. 10, 2024; accepted for publication Nov. 4, 2024

Abstract *Cyclotella cryptica*, a model diatom known for its robust adaptability to variable salinity and temperature conditions, is a promising candidate for large-scale biotechnological applications. Nutrient availability, particularly nitrogen and phosphorus, plays a crucial role in the metabolic activities of microalgae, influencing its industrial utility. Exploring the relationship between these essential nutrients and both the yield and biochemical composition of this microalga is crucial for optimizing cultivation strategies. However, research focusing on the effects of nitrogen and phosphorus on *C. cryptica* remains limited. We investigated the impacts of varying concentrations of nitrate (0.25–3.96 mmol/L) and phosphate (14.4–229.6 μmol/L) on *C. cryptica* culture by analyzing its growth performance, photosynthetic activity, biochemical composition, and biosilica deposition. Results indicate that *C. cryptica* exhibited enhanced growth, photosynthetic efficiency, and carotenoid production under higher nutrient concentrations. However, the effects of nitrate on macronutrients composition and fatty acids profile differed from those of phosphate. Specifically, increased nitrate levels resulted in higher concentrations of polyunsaturated fatty acids (PUFAs) at the expense of saturated fatty acids (SFAs), while increased phosphate levels were associated with increased PUFAs and reduced monounsaturated fatty acids (MUFAs). Additionally, biosilica deposition was weakened by elevated nitrate but enhanced by increased phosphate levels. This study improved our understanding of nutrient-mediated regulatory mechanisms in diatoms and contributed valuable data to the broader field of algal biotechnology. Moreover, these findings are expected to advance the development of tailored nutrient management strategies, thereby enhancing the industrial potential of *C. cryptica*.

Keyword: *Cyclotella cryptica*; nitrate; phosphate; fucoxanthin; frustule

1 INTRODUCTION

Microalgae encompass a wide array of both prokaryotic (e.g., Cyanophyta) and eukaryotic (e.g., Chlorophyta and Bacillariophyta) taxa, thriving in diverse aquatic environments such as lakes, rivers, and oceans. These organisms are highly valued for their prolific capacity to produce a diverse range of bioproducts, including polysaccharides, lipids, pigments, proteins, vitamins, and bioactive compounds. Additionally, the integration of

* Supported by the National Natural Science Foundation of China (No. 31902370), the Ningbo Public Welfare Science and Technology Program (No. 2022S161), and the Zhejiang Provincial Natural Science Foundation of China (No. LY22C190001)

** Corresponding author: hanjichang@nbu.edu.cn

microalgae cultivation with wastewater treatment and carbon dioxide sequestration from flue gases plays a significant role in enhancing environmental sustainability (Han et al., 2018; Zhu et al., 2020). Therefore, numerous species of microalgae have been extensively studied for their potential applications in various industries, including biofuel production, pharmaceuticals, nutraceuticals, and environmental remediation. However, transition from pilot-scale to industrial-scale production encounters multiple challenges that must be carefully addressed to fully harness the microalgae-based technologies.

Open pond systems (OPSs) are currently the predominant method for large-scale microalgae cultivation, accounting for approximately 95% of global production (Kumar et al., 2015). These systems are primarily favored for their cost-effectiveness and high productivity. Despite these advantages, OPSs are subject to significant daily fluctuations in salinity and temperature, which critically affect both the yield and quality of microalgae cultivation. For instance, in desert regions, the daily evaporation rate in OPSs can reach approximately 0.2 L/(m^2·h), which potentially doubles the salinity of the cultures within four days (Cooney et al., 2011). Temperature fluctuations in these systems can also be substantial, with variations of up to 10 °C reported (Ras et al., 2013; Khan et al., 2018). To mitigate these environmental challenges, engineering strategies such as salinity adjustment through the addition of freshwater or salt, and temperature control via heating or cooling systems are employed. However, these strategies inevitably lead to increased consumption of freshwater and energy, thereby raising operational costs. Given these challenges, there is a pressing need to explore and develop microalgae strains that can withstand a broader range of salinity and temperature conditions. Such strains would not only ensure stable productivity and quality but also help minimize the associated costs of cultivation.

Cyclotella cryptica, a model diatom species, has demonstrated substantial resilience under varying salinity conditions and strong tolerance to a broad temperature range. These characteristics enhance its adaptability and reduce the need for stringent environmental controls, potentially lowering industrial production costs. Furthermore, this microalga holds considerable promise due to its versatile applications. Notably, its ash-free dry cell weight (DCW) has been reported to reach up to 20.0 and 29.7 g/(m^2·d) in 2.8- and 48-m^2 OPSs, respectively (Laws et al., 1988; Huesemann et al., 2009). Additionally, *C. cryptica* is particularly valuable in the pharmaceutical and nutraceutical industries for its ability to accumulate various bioactive compounds, including omega-3 fatty acids (FAs) and fucoxanthin, which are renowned for their numerous health benefits. A study identified *C. cryptica* as one of the leading sources for eicosapentaenoic acid (EPA, C20:5) production among 175 microalgal strains (Slocombe et al., 2015). Moreover, the silica-based cell wall (frustule) of *C. cryptica* offers significant potential for applications in hemorrhage control and drug delivery, underscoring its value as a biomaterial (Wang et al., 2023; Yang et al., 2023). The completion of the genome sequence of *C. cryptica* and the development of various genetic engineering tools further position this microalga as an excellent candidate for the production of both natural and engineered substances (Dunahay et al., 1995; Traller et al., 2016). Collectively, these factors underscore the suitability of *C. cryptica* for scaled-up cultivation aimed at enhancing its growth performance and productivity of bioactive substances.

Like all microalgal species, the growth rate and biochemical composition of *C. cryptica* are significantly influenced by nutrient availability and various abiotic factors. For example, environmental variables such as the partial pressure of CO_2 and light intensity have been shown to substantially affect the specific growth rate, biomass concentration, lipid content, FAs profile, and chitin productivity of *C. cryptica* (Sriharan et al., 1991; Ozkan and Rorrer, 2017a, b). Increases in the nitrogen to silicon ratio (N/Si molar ratio ranging from 0.82 to 8.6) corresponded with heightened cell density and chitin yield in *C. cryptica*, thereby enhancing the peak rate of volumetric chitin productivity (Chiriboga and Rorrer, 2018). Consequently, exploring the responses of *C. cryptica* to crucial factors is essential for maximizing both biomass and bioactive substance production.

Nitrogen and phosphorus are indispensable for the metabolic and cellular functions of diatoms. Nitrogen, second only to carbon, constitutes approximately 1%–10% of the DCW in microalgal cells, playing a fundamental role in the biosynthesis of proteins, lipids, and carbohydrates (Lu et al., 2024). Phosphorus is critical for energy-related

processes, including adenosine triphosphate (ATP) and nicotinamide adenine dinucleotide phosphate (NADP) synthesis, as well as for the formation of nucleic acids and membrane phospholipids. Notably, in phosphorus-deficient environments, diatoms have developed a mechanism termed luxury uptake, which allows them to store excess phosphate for future needs (Brembu et al., 2017; Cañavate et al., 2017). The understanding of nitrogen and phosphorus metabolism in diatoms has primarily been derived from studies on model species such as *Thalassiosira pseudonana* and *Phaeodactylum tricornutum*. Research focusing on these species has extensively examined the effects of nutrient availability on metabolic regulation using diverse methodologies, including transcriptomics, metabolomics, proteomics, and classical biochemistry (Chauton et al., 2013; Yang et al., 2014; Feng et al., 2015; Cañavate et al., 2017; Alipanah et al., 2018). These studies underscore that variations in nitrogen and phosphorus availability significantly influence diatom metabolism, affecting growth rates, the distribution of carbon flow among macronutrients, and the content of bioactive components. Such insights are crucial for optimizing cultivation strategies to enhance the productivity and biochemical profiles of these diatom species.

Despite the availability of a published genome sequence and its potential for various industrial applications, research into the impacts of nitrogen and phosphorus on the metabolic regulation of *C. cryptica* and related species remains limited. Previous studies have primarily focused on the effects of nitrogen concentrations, particularly under conditions of nitrogen deficiency, and the impact of different nitrogen sources on the growth performance of *C. cryptica*. However, these studies have largely overlooked the changes in biochemical composition in response to varying nitrogen conditions (Liu and Hellebust, 1974; Shifrin and Chisholm, 1981; Sriharan et al., 1991; Pahl et al., 2012). Similar situation has been observed in phosphorus-related research. For example, Chiriboga and Rorrer (2019) developed phosphate addition strategies to enhance lipid and chitin nanofiber productivity in *Cyclotella* sp., but did not assess the impact of phosphate on other value-added compounds such as fucoxanthin, EPA, and frustules. Moreover, Tilman and Kilham (1976) explored the growth rates of *C. meneghiniana* under various phosphate levels but did not report on any corresponding changes in biochemical composition. This research gap significantly hinders the optimization of cultivation systems for *C. cryptica*, impacting the ability to fully exploit its industrial potential.

The objective of this study was to investigate the effects of varying nitrate and phosphate concentrations on *C. cryptica*, specifically focusing on its growth performance, photosynthetic activity, macronutrient composition, production of value-added substances, and biosilica deposition. Given the notable gaps in the literature regarding the biogenesis of frustules under different nutrient conditions, this research also explored the transcriptional regulation of five genes (*CcSin1*, *CcSin2*, and *CcSAP1–3*) encoding silicalemma transmembrane proteins using quantitative reverse transcription-PCR (qRT-PCR). Insights gained from this study are expected to deepen our understanding of the adaptive responses of *C. cryptica* to variations in phosphate and nitrate levels, thereby aiding the development of optimized cultivation practices for large-scale applications.

2 MATERIAL AND METHOD

2.1 *Cyclotella cryptica* strain and cultivation conditions

Cyclotella cryptica NMBdh11-05 used in this study was sourced from the Microalgae Collection Center at Ningbo University. Cultivation occurred under controlled environmental conditions: temperature was maintained at 25±2 °C and illumination was provided by white fluorescent lighting at an intensity of approximately 45 photons/(m^2·s), following a 12-h:12-h light:dark photoperiod.

The basic medium used in this study was NMB3#, to which 0.1-mmol/L sodium metasilicate nonahydrate ($Na_2SiO_3·9H_2O$) was added as per the concentrations reported by Hsieh et al. (1985). This formulation comprises nitrate and phosphate at molar concentrations of 0.99 mmol/L and 57.4 μmol/L, respectively. These concentrations represent approximately 56% and 80% of those found in f/2 medium, which contains 1.76-mmol/L nitrate and 71.4-μmol/L phosphate (Fang et al., 2024). Initial salinity was maintained at 25, and pH was adjusted to 8.0.

Cells pre-cultured to the early stationary phase in 1×NMB3# medium were inoculated into fresh NMB3# medium with varying concentrations of nitrate and phosphate. An inoculation ratio of 1:9 (algal culture to fresh medium) was consistently

maintained. The gradient of nitrate and phosphate concentrations tested included 1/4, 1/2, 1, 2, and 4 times the standard concentration found in NMB3# medium. Specifically, nitrate concentrations were adjusted to 0.25, 0.49, 0.99, 1.98, and 3.96 mmol/L, and phosphate concentrations to 14.4, 28.7, 57.4, 114.8, and 229.6 μmol/L, with the standard 1× NMB3# medium serving as the control. Cultivation was conducted in 500-mL conical flasks, each containing 200 mL of medium.

2.2 Evaluation of growth performance and photosynthetic activity

The cell density of *C. cryptica* cultures was monitored bi-daily by measuring the optical density at 750 nm (OD_{750}) using a Varioskan™ LUX spectrophotometer (Thermo Fisher Scientific, USA). The specific growth rate (μ, /d) was calculated from these OD_{750} measurements using a method previously described (Sun et al., 2022). Additionally, the maximal photosystem II (PSII) quantum yield (F_v/F_m) was tested every two days to represent the photosynthetic activity by WATER-PAM (WALZ, Germany).

At the end of the cultivation period (12 d), 10-mL samples of the microalgal culture were filtered through pre-weighed Whatman GF/F microfiber filters with a pore size of 0.7 μm. Filters were washed three times with ultrapure water and dried at 60 °C for 48 h until a constant weight was achieved. The DCW was then gravimetrically determined by comparing the weights of the filters before and after the filtration of the microalgal cells.

2.3 Identification of macronutrients composition

Cyclotella cryptica cells were harvested on the 12th day and collected via centrifugation at 3 220×*g* for 10 min. The resultant cell pellets were thoroughly washed three times with ultrapure water and subsequently freeze-dried to prepare for biochemical analysis.

The protein content was determined based on Coomassie brilliant blue G250 method (Sedmak and Grossberg, 1977). First, approximately 10-mg portion of lyophilized powder was mixed with 1 mL of protein extraction buffer composed of 50-mmol/L Tris-HCl (pH 7.4), 150-mmol/L NaCl, 1-mmol/L EDTA, 1-mmol/L phenylmethylsulfonyl fluoride, and 1% (v/v) Triton X-100. The sample was then incubated in an ice bath for 4 h to facilitate protein extraction. After incubation, the mixture was centrifuged at 13 539×*g* for 20 min at 4 °C to separate the supernatant. The supernatant, containing the extracted proteins, was carefully collected for further analysis.

For protein quantification, a 100-μL aliquot of the supernatant was mixed with 5 mL of Coomassie brilliant blue reagent and vortexed thoroughly to ensure complete mixing. After allowing the mixture to rest for 2 min, the optical density at 595 nm (OD_{595}) was measured using a spectrophotometer. The protein concentration was calculated based on a standard curve generated with bovine serum albumin.

The carbohydrate was measured utilizing the modified phenol-sulfuric acid method (Zhang et al., 2020). Approximately 10 mg of microalgal powder was mixed with 1 mL of a papain and cellulase solution in a 1∶1 ratio (v/v). The mixture was incubated in a water bath at 40 °C for 30 min, followed by boiling for 10 min and then incubating at 70 °C for 4 h. After centrifugation at 13 539×*g* for 15 min at 4 °C, the supernatant was carefully collected and mixed with 4.5 mL of 95% ethanol. This mixture was incubated for 12 h and centrifuged again at 13 539×*g* for 15 min at 4 °C. The resulting pellet was resuspended in 2 mL of deionized water and vortexed at 1 200 r/min for 1 min. After a 10-min incubation, the sample was centrifuged once more at 13 539×*g* for 15 min at 4 °C. The supernatant was then mixed with phenol (C_6H_5OH) and sulfuric acid (H_2SO_4) for 5 min, followed by boiling for 20 min and cooling in an ice bath for 10 min. Finally, the optical density at 490 nm (OD_{490}) was measured using a spectrophotometer, and the carbohydrate concentration was calculated using a glucose standard curve.

Lipids were quantified following the $CHCl_3$-CH_3OH method (Bligh and Dyer, 1959). In brief, approximately 20 mg of microalgal powder was mixed with 2 mL of $CHCl_3$-CH_3OH (1∶1, v/v) and incubated on a shaker at 26 °C and 260 r/min for 12 h. After incubation, the mixture was centrifuged at 13 539×*g* for 10 min at 4 °C, and the supernatant was carefully transferred to a glass tube. This extraction process was repeated twice for thorough lipid recovery. Subsequently, 2.5 mL of $CHCl_3$ and 4.5 mL of 1% NaCl were added to the pooled supernatants. After another centrifugation at 13 539×*g* for 10 min at 4 °C, the organic phase was collected and dried under a nitrogen stream. The final lipid extract was weighed, and lipid content was calculated based on the weight difference.

2.4 Analysis of FAs profile, and carotenoids content

For the extraction of FAs, approximately 10 mg of freeze-dried microalgal samples were treated with 3 mL of 2-mol/L KOH in methanol. This solution was vortexed vigorously and then heated at 75 °C for 30 min. Following this, 1.5 mL of 3-mol/L HCl in methanol was added, and the temperature was maintained for an additional 30 min to facilitate complete hydrolysis. Subsequently, fatty acid methyl esters (FAMEs) were extracted using n-hexane. The analysis was conducted via gas chromatography-mass spectrometry (GC-MS) on an Agilent Technologies system (Model 8890A-5977B, USA), equipped with a CD-2560 capillary column (100 m×0.25 mm×0.2 μm, CNW, Germany). Helium was utilized as the carrier gas at a flow rate of 0.81 mL/min. The temperature protocol began at 140 °C for 5 min, increased by 4 °C/min to 240 °C, and maintained at this peak for 20 min. FAs were identified and quantified based on retention times and peak areas, with verification against the NIST14.L and Wiley7 spectral databases.

Carotenoids were extracted by mixing 5 mL of chloroform/methanol (1∶1, v/v) containing 0.1% butylated hydroxy toluene with 5 mg of lyophilized algal powder. After vortexing for 5 min, the mixture was ultrasonicated for 20 min in an ice-water bath to aid in extraction. The sample was then centrifuged at 13 539×*g* for 5 min at 4 °C, and the supernatant was filtered through a 0.22-μm polytetrafluoroethylene membrane. The identification was performed using high-performance liquid chromatography (HPLC, 1260 Infinity II, Agilent, Germany) coupled with a Triple Quadrupole Mass Spectrometer (Agilent 6400 Series, USA), with quantification based on ion *m*/*z* values (mass error ≤5×10^{-6}), retention time, isotopic distribution, and MS/MS spectra.

2.5 Determination of morphology properties of the frustule and biosilica content of *C. cryptica*

A modified method was employed to analyze the biosilica content in the frustules of *C. cryptica* (Kirkham et al., 2017). Initially, approximately 5 mg of microalgal powder was suspended in 1 mL of ultrapure water. To mitigate the influence of intracellular silicate on the results, the suspension was heated to 95 °C for 1 h in a metal bath to lyse the cells and release the intracellular silicate. Subsequently, the sample was centrifuged at 3 220×*g* for 5 min. The resulting pellet was soaked in 1 mL of methanol overnight, followed by repeated methanol washes until the frustules appeared colorless. The frustules were then thoroughly rinsed with ultrapure water and centrifuged once more. The cleaned frustules were treated with 0.5-mol/L NaOH at 95 °C for an additional hour to extract the biosilica. After cooling, the solution was neutralized with 0.5-mol/L H_2SO_4 and centrifuged to remove all particulates. The optical density at 810 nm (OD_{810}) of the supernatant was measured using a Microplate Reader (Varioskan LUX, Thermo Fisher Scientific, USA), which was calibrated against a standard curve established using sodium hexafluorosilicate.

Microalgal cells harvested on Day 12 were collected by centrifugation and subsequently acidified by concentrated HCl at 100 °C for 20 min. Following acidification, the samples were thoroughly rinsed with distilled water to restore a neutral pH and then air-dried. The dried samples were mounted on aluminum stubs for examination under a Hitachi S-4800 scanning electron microscope (SEM) (Hitachi, Japan). The morphological property of valve diameter was determined based on the SEM micrographs.

2.6 Transcriptional pattern of genes related to frustule biogenesis

Microalgal cells collected on Days 4, 8, and 12 were subjected to centrifugation at 3 220×*g* for 10 min and used for total RNA isolation employing the Plant RNA Kit (Omega, USA). The integrity of the RNA was verified through agarose gel electrophoresis, and its concentration was quantified using absorbance ratios at 230 nm, 260 nm, and 280 nm with a NanoDrop ND-1000 spectrophotometer (NanoDrop, USA). Genomic DNA was removed, and cDNA synthesis was performed using the PrimeScript™ RT Reagent Kit (TaKaRa, China). The transcriptional responses of five genes (*CcSin1*, *CcSin2*, and *CcSAP1–3*) under various phosphate conditions were assessed by qRT-PCR using a BioRad system (USA). Gene expression was normalized to the internal reference gene, *Histone H4*, using the $2^{-\Delta\Delta Ct}$ method. Primer sequences (designed by Primer Premier 5) and the JGI accession numbers for all genes analyzed are listed in Table 1.

2.7 Statistical analysis

The morphological characteristics of *C. cryptica* were qualitatively assessed based on approximately ten SEM micrographs for each treatment condition.

Table 1 Primers used in this study

Gene	JGI ID	Primer
HistoneH4	g18763.t1	F: 5′-AAACCCGTGGTGTCCTCAAG-3′
		R: 5′-CGTAGACGACATCCATCGCA-3′
CcSin1	g20669.t1	F: 5′-TGACGGTTACGTTGAGGTCG-3′
		R: 5′-GTTCTTGTTGCCCTGTTCGC-3′
CcSin2	g25218.t1	F: 5′-CTGTCTTGCGATTCAAGCGG-3′
		R: 5′-CTGTCTTGCGATTCAAGCGG-3′
CcSAP1	g14294.t1	F: 5′-GGAAAGGCGGGAGTTCCAGTT-3′
		R: 5′-ATGACACAGCGTTCGGGTTCA-3′
CcSAP2	g8103.t1	F: 5′-GAGACGACGATGCCAACTGT-3′
		R: 5′-GCCCCATCCACTGCTACTTG-3′
CcSAP3	g9622.t1	F: 5′-CCTCCTCTTCCTCCTCCAACCA-3′
		R: 5′-GACAACCCGTCGACGTGACTT-3′

For other measured parameters, analyses were performed on three biological replicates. Statistical differences among treatments under different conditions were determined using one-way ANOVA with a significance level set at $P<0.05$. The Least Significant Difference (LSD) post hoc test was employed to identify significant variations. All statistical analyses were conducted using SPSS Statistics 25.0. Results are presented in mean± standard deviation (SD).

3 RESULT

3.1 Growth performance and photosynthetic activity of *C. cryptica* under different nitrogen and phosphate regimes

Three parameters including OD_{750}, specific growth rate, and final biomass concentration were adopted in this study to evaluate the growth performances of *C. cryptica*. As illustrated in Fig.1a, the cell densities of *C. cryptica* showed significant increases with elevated initial nitrate concentrations. The lowest final OD_{750} (0.06) was observed at a nitrate concentration of 0.25 mmol/L. As the nitrate concentration was raised to 0.49 and 0.99 mmol/L, OD_{750} correspondingly increased to 0.09 and 0.15,

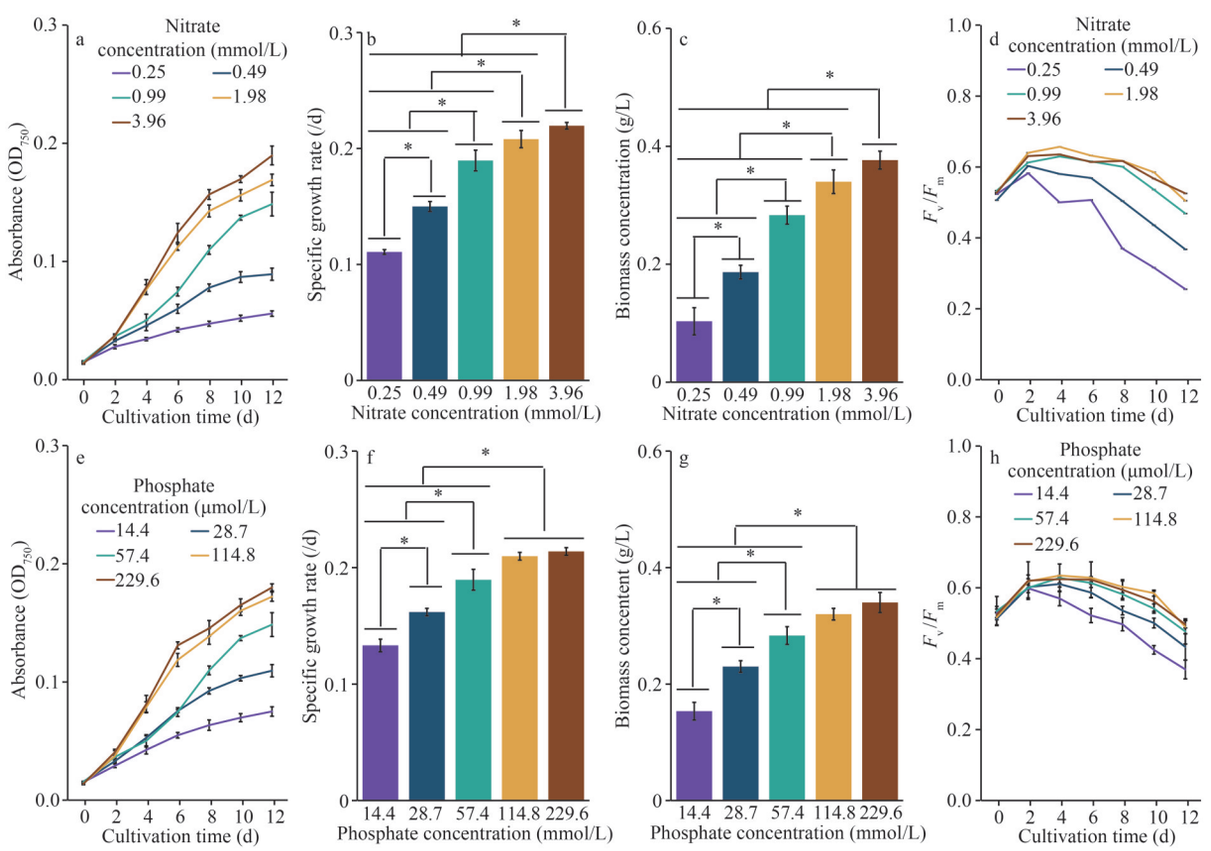

Fig.1 Growth performance and photosynthetic activity of *C. cryptica* across varying concentrations of nitrate and phosphate

a–d. nitrate treatments detailing cell density, specific growth rate, biomass concentration, and F_v/F_m; e–h. the same parameters under phosphate treatments. Data are presented as mean±SD (n=3); *: indicates significant differences ($P<0.05$).

respectively. Further augmentations to 1.98 and 3.96 mmol/L led to additional enhancements in OD_{750}; however, these increases were not as pronounced as those observed during the earlier rise from 0.49 to 0.99 mmol/L. The specific growth rates, depicted in Fig.1b, experienced a sharp ascent from 0.11/d at 0.25 mmol/L to 0.22/d at 3.96 mmol/L. Initially, the increase was marked within the nitrate range of 0.25–0.99 mmol/L and then transitioned to a more tempered rise from 0.99 to 3.96 mmol/L, a trend that was similar to the pattern noted in cell density. The biomass content, as detailed in Fig.1c, similarly tracked the trends seen in specific growth rates. Concerning photosynthetic activity, the F_v/F_m in treatments receiving 0.25- and 0.49-mmol/L nitrate demonstrated a consistent decline commencing on the second day, culminating in final values of approximately 0.26 and 0.37, respectively. Although the remaining three treatments also initially exhibited an increase followed by a decrease in F_v/F_m values, these values remained relatively stable from Day 2 to Day 8 (Fig.1d). The response of *C. cryptica* to phosphate treatments was similar to that observed for nitrate treatments, with the exception that no significant differences were detected in specific growth rate or biomass content between the two highest phosphate concentrations (Fig.1e–h). Specifically, the group exposed to the lowest phosphate concentration of 14.4 μmol/L exhibited the minimal values in OD_{750}, specific growth rate, biomass content, and F_v/F_m. In contrast, the group treated with the highest phosphate concentration (229.6 μmol/L) demonstrated the highest values for these parameters.

3.2 Macromolecular composition of *C. cryptica* under different nitrate and phosphate concentrations

Alterations in both nitrate and phosphate concentrations had a significant impact on the biochemical composition of *C. cryptica*, while the response patterns to these two nutrients differed distinctly. Specifically, an increase in nitrate concentrations from 0.25 to 3.96 mmol/L resulted in a notable increase in protein contents from 17.7% to 38.5% of DCW, while lipid and carbohydrate contents decreased from 32.5% and 12.7% of DCW to 16.0% and 7.2% of DCW, respectively (Fig.2a–c). In contrast, elevated phosphate concentrations were correlated with a substantial rise in carbohydrate levels. For example, the carbohydrate content at a phosphate concentration of 229.6 μmol/L was 1.7 times of that observed at 14.4 μmol/L (Fig.2d). The lipid contents decreased with rising phosphate concentrations, following a trend akin to that observed with increasing nitrate levels (Fig.2e). Protein levels increased with phosphate concentrations up to 57.4 μmol/L and then stabilized between 57.4–229.6 μmol/L (Fig.2f).

3.3 The influence of varied nitrate and phosphate on FAs profile and carotenoids composition of *C. cryptica*

In this study, we identified 11 types of FAs in *C. cryptica*, including three saturated fatty acids (SFAs), two monounsaturated fatty acids (MUFAs), and six polyunsaturated fatty acids (PUFAs). Our data revealed that changes in nitrate and phosphate concentrations significantly influenced the FAs profile and carotenoids composition.

As depicted in Table 2, the concentrations of palmitic acid (PA, C16:0), hexadecadienoic acid (HDDA, C16:2), hexadecatrienoic acid (HTA, C16:3), stearic acid (SA, C18:0), and oleic acid (OA, C18:1) varied significantly in response to different nitrate concentrations. Contents of HDDA, HTA, and OA were found to be positively correlated with increasing levels of nitrate, exhibiting a marked upward trend. Conversely, PA concentrations were inversely related to nitrate levels. Specifically, at a nitrate concentration of 0.25 mmol/L, the proportions of HDDA and HTA were relatively low, at approximately 0.7% and 3.3% of total fatty acids (TFAs), respectively. These proportions increased significantly to 7.8%–9.8% for HDDA and 7.0%–10.7% for HTA in treatments with higher nitrate levels. In contrast, treatments with high nitrate concentrations ranging from 0.49 to 3.96 mmol/L were characterized by significantly reduced SA content, consistently below 1.0% of TFAs. Notably, cells exposed to 0.25-mmol/L nitrate exhibited a SA proportion of 8.7% of TFAs. Regarding other SFAs, PA followed a variation trend similar to SA, indicating a considerable decrease in concentration with higher nitrate levels, while myristic acid (MA, C14:0) varied within a relatively narrow range across all tested nitrate concentrations. EPA contents increased from 11.0% to 17.6% of TFAs for nitrate treatments within 0.25–0.99 mmol/L, but then decreased to 10.6%–15.3% in the nitrate treatments of 1.98 and 3.96 mmol/L. Palmitoleic acid (POA, C16:1), a dominant FA in *C. cryptica*, peaked at a nitrate concentration of 0.25 mmol/L and reached its lowest level at 0.99 mmol/L, showing significant

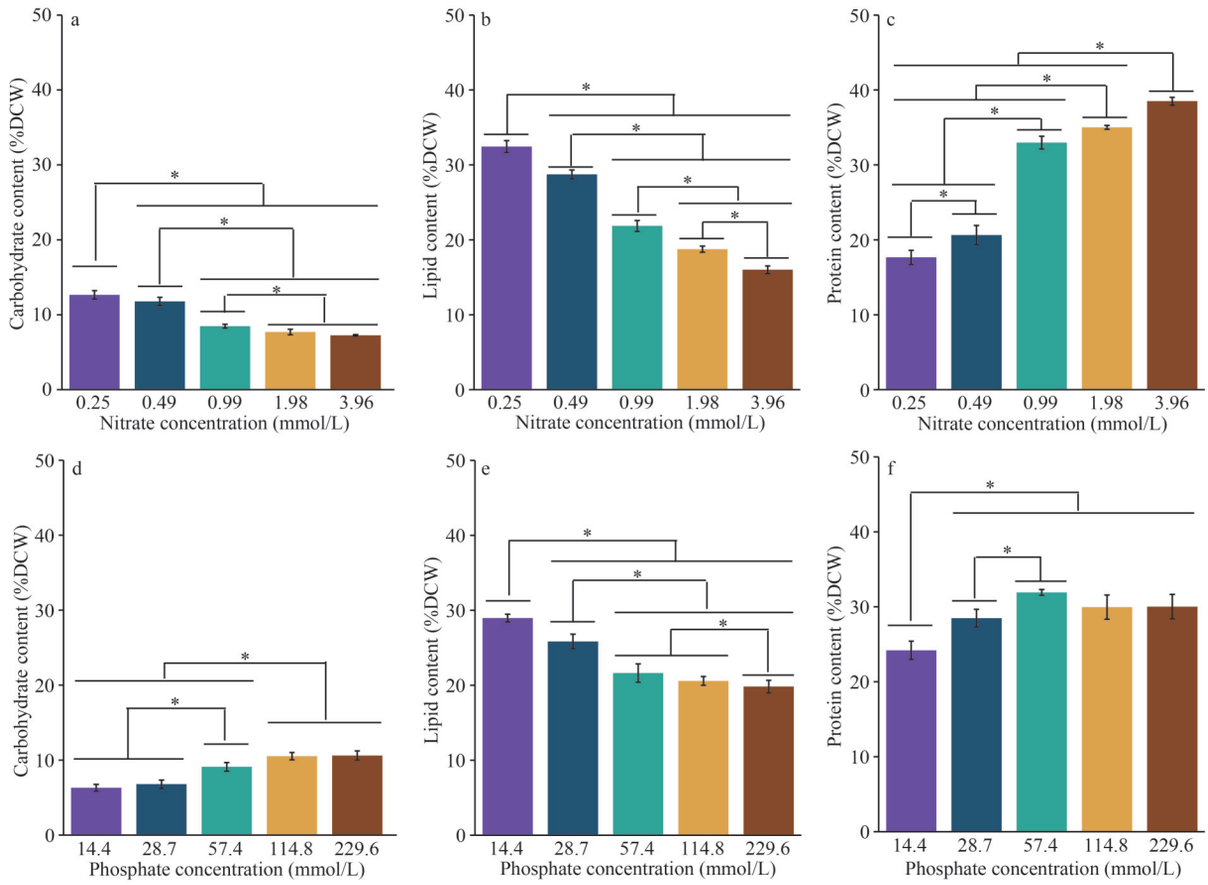

Fig.2 Macronutrient profiles of *C. cryptica* at varying nitrate and phosphate concentrations

a–c & d–f. corresponding to carbohydrate, lipid, and protein content under nitrate and phosphate treatments, respectively. Data are presented as mean±SD (n=3); *: denotes significant differences (P<0.05); DCW: dry cell weight.

variability but no discernible correlation with nitrate levels. The specific FA variations further significantly influenced the overall profiles of SFAs, MUFAs, and PUFAs. SFAs displayed a clear downward trend with increasing nitrate concentrations, with the highest proportion, 51.1% of TFAs, observed at 0.25-mmol/L nitrate. In contrast, the proportions of SFAs in treatments with nitrate concentrations from 0.99 to 3.96 mmol/L averaged around 30.0% of TFAs. Additionally, the nitrate treatments of 1.98 and 3.96 mmol/L exhibited significantly higher MUFAs proportions compared to the three lower nitrate groups. PUFAs showed a bell-shaped distribution pattern, peaking at 43.5% of TFAs at a nitrate concentration of 0.99 mmol/L.

In contrast to nitrate, enhanced phosphate concentrations led to an increase in PUFAs and a decrease in MUFAs, while having minimal effects on SFAs (Table 3). Specifically, the percentages of three SFAs, i.e., MA, PA, and SA, ranged 8.3%–9.2%, 21.8%–24.3%, and 0.8%–1.1% of TFAs, respectively, among five phosphate treatments. In the case of MUFAs, POA exhibited a sharp decline from 34.9% of TFAs at a phosphate concentration of 14.4 μmol/L to 21.0% at 57.4 μmol/L, stabilizing subsequently in treatments with 114.8 and 229.6 μmol/L of phosphate. In contrast, OA peaked at a phosphate concentration of 28.7 μmol/L, maintaining similar levels at 114.8 and 229.6 μmol/L but significantly exceeding those observed at 14.4 and 57.4 μmol/L. Among the six analyzed PUFAs, HDDA, linoleic acid (LA, C18:2), EPA, and docosahexaenoic acid (DHA, C22:6) increased with higher phosphate concentrations, whereas HTA and arachidonic acid (AA, C20:4) showed opposite trends. Notably, the proportion of EPA reached its maximum at a concentration of 114.8 μmol/L, displaying negligible differences with the concentrations of 57.4 and 229.6 μmol/L, yet approximately three times higher than that at 14.4 μmol/L.

As for the pigments, only fucoxanthin and diadinoxanthin, the two predominant carotenoids in

Table 2 FAs and carotenoids of *C. cryptica* under different nitrate levels

Parameter	Nitrate concentration (mmol/L)				
	0.25	0.49	0.99	1.98	3.96
Fatty acid (%TFAs)					
MA (C14:0)	9.3±0.3^{a}	8.2±0.4^{b}	9.2±0.5^{a}	7.6±0.1^{c}	8.4±0.1^{b}
PA (C16:0)	33.0±0.7^{a}	28.4±0.7^{b}	21.0±0.2^{c}	19.1±0.4^{d}	20.2±0.4^{c}
POA (C16:1)	25.9±0.2^{a}	23.1±0.4^{d}	19.9±0.4^{e}	25.1±0.4^{b}	24.0±0.5^{c}
HDDA (C16:2)	0.7±0.4^{d}	7.8±0.4^{c}	8.5±0.9^{bc}	8.8±0.4^{b}	9.8±0.3^{a}
HTA (C16:3)	3.3±0.9^{d}	7.0±1.0^{c}	9.7±0.3^{ab}	8.7±0.2^{b}	10.7±0.1^{a}
SA (C18:0)	8.7±0.6^{a}	0.9±0.0^{b}	0.8±0.0^{b}	0.9±0.0^{b}	0.6±0.0^{b}
OA (C18:1)	2.5±0.6^{c}	4.9±0.4^{b}	5.6±0.9^{b}	8.9±0.1^{a}	9.3±0.2^{a}
LA (C18:2)	0.6±0.1^{c}	1.1±0.0^{b}	1.0±0.1^{b}	1.2±0.2^{b}	1.4±0.2^{a}
AA (C20:4)	2.9±0.2^{b}	3. 6± 0.0^{a}	1.4±0.2^{d}	2.4±0.0^{c}	2.8±0.1^{b}
EPA (C20:5)	11.0±0.4^{c}	11.9±0.6^{c}	17.6±0.9^{a}	15.3±0.1^{b}	10.6±1.2^{c}
DHA (C22:6)	2.0±0.3^{c}	3.1±0.1^{b}	5.4±0.3^{a}	2.2±0.0^{c}	2.1±0.1^{c}
SFA	51.1±0.9^{a}	37.5±0.7^{b}	31.0±0.5^{c}	27.5±0.4^{e}	29.2±0.5^{d}
MUFA	28.4±0.7^{b}	28.0±0.8^{b}	25.5±1.3^{c}	34.1±0.3^{a}	33.3±0.7^{a}
PUFA	20.5±1.6^{d}	34.5±0.5^{c}	43.5±1.6^{a}	38.4±0.6^{b}	37.6±0.9^{b}
Carotenoid (mg/g of DCW)					
Fucoxanthin	1.9±0.1^{d}	3.4±0.2^{c}	7.3±0.4^{b}	7.8±0.2^{a}	7.8±0.2^{a}
Diadinoxanthin	0.2±0.0^{c}	0.4±0.0^{b}	1.0±0.1^{a}	1.0±0.1^{a}	1.0±0.1^{a}

Values are displayed as mean±SD (n=3). TFAs: total fatty acids; PA: palmitic acid; HDDA: hexadecadienoic acid; HTA: hexadecatrienoic acid; SA: stearic acid; OA: oleic acid; MA: myristic acid; POA: palmitoleic acid; LA: linoleic acid; AA: arachidonic acid; EPA: eicosapentaenoic acid; DHA: docosahexaenoic acid; SFA: saturated fatty acid; MUFA: monounsaturated fatty acid; PUFA: polyunsaturated fatty acid; DCW: dry cell weight. Different letters of superscripts in the same row indicate statistically significant difference between groups (P< 0.05). Groups with no superscript indicate no significant differences.

Table 3 FAs and carotenoids of *C. cryptica* under different phosphate levels

Parameter	Phosphate concentration (μmol/L)				
	14.4	28.7	57.4	114.8	229.6
Fatty acid (%TFAs)					
MA (C14:0)	9.0±0.3	8.3±0.9	9.2±0.5	8.7±0.5	8.4±0.9
PA (C16:0)	21.9±1.1^{b}	24.3±1.1^{a}	21.0±0.2^{b}	21.9±0.6^{b}	21.8±0.5^{b}
POA (C16:1)	34.9±0.2^{a}	23.3±0.9^{b}	19.9±0.4^{c}	19.1±0.7^{c}	19.4±1.2^{c}
HDDA (C16:2)	6.1±0.1^{c}	7.3±0.3^{b}	8.5±0.9^{a}	8.6±0.6^{a}	9.2±0.1^{a}
HTA (C16:3)	10.7±0.3^{a}	9.2±0.1^{b}	9.7±0.3^{b}	6.1±0.4^{c}	6.1±0.1^{c}
SA (C18:0)	0.9±0.1^{b}	1.0±0.0^{a}	0.8±0.0^{b}	1.1±0.1^{a}	1.0±0.1^{ab}
OA (C18:1)	5.6±0.8^{b}	9.2±0.2^{a}	5.6±0.9^{b}	8.2±0.4^{a}	8.9±0.2^{a}
LA (C18:2)	ND^{c}	1.0±0.2^{b}	1.0±0.1^{b}	1.4±0.3^{a}	1.6±0.2^{a}
AA (C20:4)	2.5±0.2^{a}	2.4±0.1^{a}	1.4±0.2^{b}	1.2±0.2^{b}	1.1±0.2^{b}
EPA (C20:5)	6.7±0.3^{c}	10.5±0.5^{b}	17.6±0.9^{a}	18.2±0.8^{a}	17.6±1.2^{a}
DHA (C22:6)	1.8±0.1^{c}	3.4±0.6^{b}	5.4±0.3^{a}	5.6±0.2^{a}	5.0±0.2^{a}
SFA	31.7±0.8^{b}	33.7±0.5^{a}	31.0±0.5^{b}	31.7±0.4^{b}	31.2±0.6^{b}
MUFA	40.5±0.6^{a}	32.4±1.1^{b}	25.5±1.3^{d}	27.3±0.6^{c}	28.4±1.2^{c}
PUFA	27.8±0.2^{d}	33.9±1.0^{c}	43.5±1.6^{a}	41.0±0.5^{b}	40.4±1.2^{b}
Carotenoid (mg/g of DCW)					
Fucoxanthin	3.7±0.4^{b}	7.0±0.3^{a}	7.3±0.4^{a}	7.6±0.4^{a}	6.9±0.7^{a}
Diadinoxanthin	0.5±0.1^{b}	0.7±0.2^{b}	1.0±0.1^{ab}	0.8±0.2^{b}	1.1±0.2^{a}

Values are displayed as mean±SD (n=3). TFA: total fatty acids; PA: palmitic acid; HDDA: hexadecadienoic acid; HTA: hexadecatrienoic acid; SA: stearic acid; OA: oleic acid; MA: myristic acid; POA: palmitoleic acid; LA: linoleic acid; AA: arachidonic acid; EPA: eicosapentaenoic acid; DHA: docosahexaenoic acid; SFA: saturated fatty acid; MUFA: monounsaturated fatty acid; PUFA: polyunsaturated fatty acid; DCW: dry cell weight; ND: not detected. Different letters of superscripts in the same row indicate statistically significant difference between groups (P<0.05). Groups with no superscript indicate no significant differences.

C. cryptica, were quantified in this study. As shown in Fig.3, fucoxanthin and diadinoxanthin were detected at retention times of approximately 2.5 min and 3.6 min, respectively. The identification of these compounds was further validated by mass spectrometric data, with m/z values of 659.429 3 and 583.412 1, respectively.

Generally, the response of carotenoids to nitrate closely mirrored their response to phosphate. With increasing nitrate concentrations from 0.25 to 0.99 mmol/L, both fucoxanthin and diadinoxanthin demonstrated a positive correlation, marked by substantial increases, before plateauing at higher concentrations ranging from 0.99 to 3.96 mmol/L (Table 2). Specifically, at the initial nitrate level of 0.25 mmol/L, fucoxanthin and diadinoxanthin concentrations were 1.9 and 0.2 mg/g, respectively; these values escalated to 7.3 and 1.0 mg/g at 0.99 mmol/L, representing approximately four-fold and five-fold increases. However, further increases in nitrate concentration to 1.98 and 3.96 mmol/L did not induce significant changes in the concentrations of these carotenoids, remaining consistent with levels observed at 0.99 mmol/L. Similarly, fucoxanthin showed an initial increase followed by a stable variation pattern with increasing phosphate concentrations, starting at a minimum of 14.4 μmol/L and peaking at 114.8 μmol/L. Diadinoxanthin levels across varying phosphate concentrations fluctuated similarly to fucoxanthin (Table 3).

3.4 Effect of nitrate and phosphate on the frustule properties of *C. cryptica*

The frustule of *C. cryptica* possesses two interconnected circular valves framed by girdle bands. Each valve is distinguished by an outer

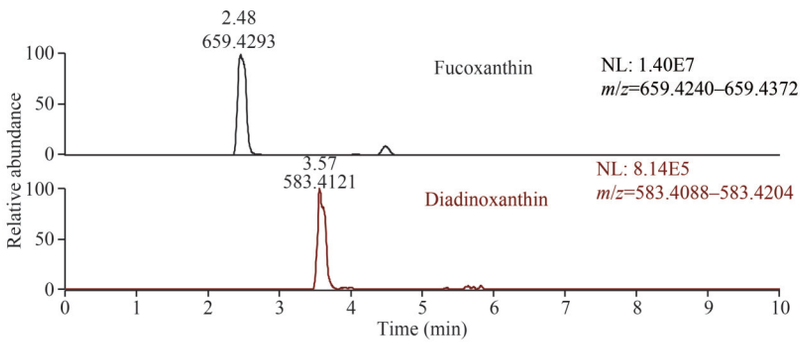

Fig.3 HPLC chromatogram and mass spectrometric identification of fucoxanthin and diadinoxanthin in *C. cryptica*

NL: normalized level; *m*/*z*: mass-to-charge ratio.

(distal) and an inner (proximal) surface. The outer surface is notable for its areolae formations (Fig.4a), which include sizeable, variably shaped foramina and cribrum pores. Conversely, the inner surface displays cribrum pores that are round and evenly spaced in radial configurations, delineated by costae (Fig.4a′). Additionally, both valve faces are marked by the presence of central fultoportulae (Fig.4b & b′) and peripheral rimoportulae (Fig.4c & c′).

Despite maintaining their characteristic round shape under various experimental conditions, frustules displayed significant abnormalities in fultoportulae, rimoportulae, and silicification extent at both the lowest (1/4×NMB3#, equivalent to 0.25-mmol/L nitrate and 14.4-μmol/L phosphate) and highest (4×NMB3#, corresponding to 3.96-mmol/L nitrate and 229.6-μmol/L phosphate) concentration conditions. Notably, several frustules from these extreme concentrations lacked fultoportulae entirely (Fig.4d–i & d′–i′). Displacement of rimoportulae from the periphery toward the center was a prevalent feature in the majority of frustules subjected to the lowest concentration treatments (Fig.4d, 4e, 4d′, & 4e′). In one instance, a frustule at the lowest nitrate level exhibited two rimoportulae located adjacently (Fig.4d′). For the frustules from the treatment of the lowest phosphate concentration, the areolae structures on the distal valve were too

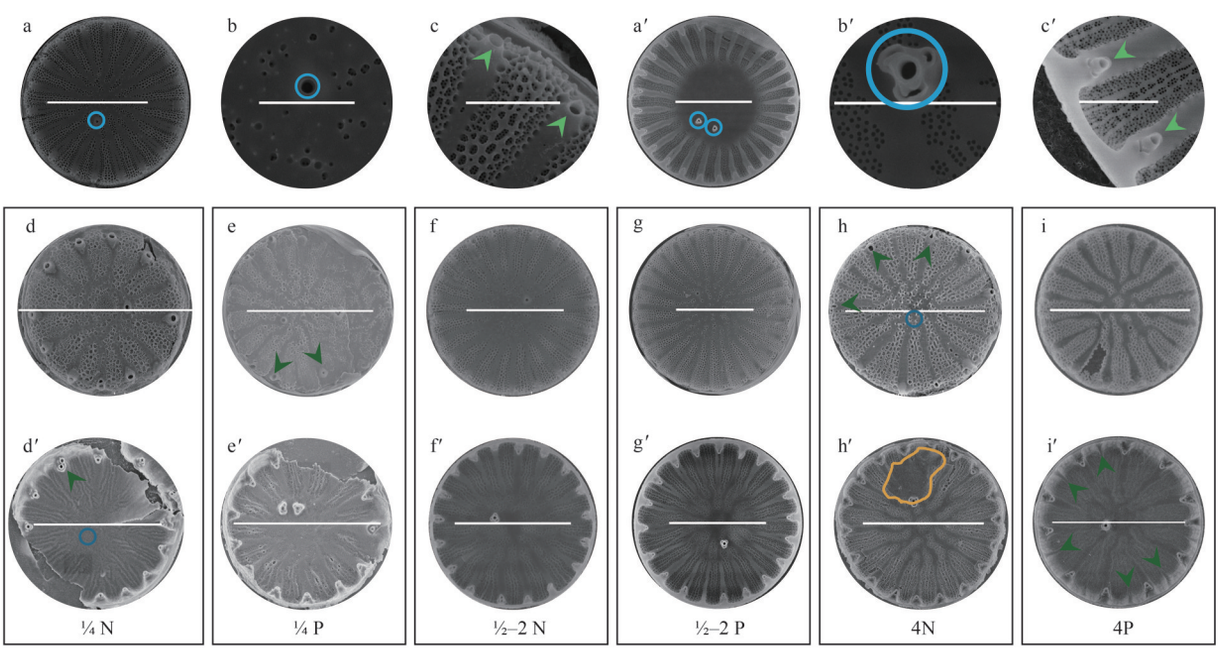

Fig.4 SEM micrographs of *C. cryptica* under varying nitrate and phosphate concentrations

a & a′. the proximal and distal valves; d, d′, e, & e′. conditions at 1/4×concentration; f, f′, g, & g′. conditions at (1/2–2)×concentration; h, h′, i, & i′. conditions at 4×concentration. Cyan circles and green arrowheads highlight normal fultoportulae and rimoportulae, while deep cyan circles and dark green arrowheads or ellipses show abnormalities in these structures. Yellow curves delineate regions without cribrum pores. Scale bars: 1 μm in (b, b′, c, and c′); 5 μm in others.

blurry to discern clearly (Fig.4e). Moreover, the costae and cribrum pores on the proximal valve were misaligned, appearing on different planes and suggesting an incomplete formation of the cribrum plate (Fig.4e′). These findings indicated that the silicification of the frustules was severely compromised by phosphate deficiency. In contrast, frustules exposed to mid-range nutrient concentrations (1/2–2) ×NMB3# displayed flat proximal and distal surfaces without noticeable morphological anomalies (Fig.4f, 4g, 4f′, & 4g′). Furthermore, in a frustule subjected to the highest nitrate concentration (4×NMB3#), an area typically occupied by cribrum pores was instead filled with solid silica panels (Fig.4i′).

To further elucidate the effects of variable nitrate and phosphate concentrations on biosilica deposition in *C. cryptica*, quantitative analyses were also performed focusing on valve diameter and biosilica content.

As shown in Table 4, the investigation revealed that the valve diameters of *C. cryptica* frustules exhibited a bell-shaped response to the incremental concentrations of nitrate and phosphate. Among all nitrate concentrations, the peak valve diameter was 11.2 μm under a nitrate concentration of 1.99 mmol/L, whereas a marginally lesser diameter of 10.1 μm was at a concentration of 0.98 mmol/L. Correspondingly, in phosphate treatments, the most substantial valve diameter was observed at a concentration of 57.4 μmol/L (1×NMB3#), and the 2×NMB3# concentration showed only a slightly reduced diameter. In stark contrast, frustules exposed to either markedly high or low concentrations of nitrate and phosphate demonstrated significant reductions in valve diameter.

The impact of varied nitrate concentrations on biosilica content was distinct from that observed with phosphate (Table 4). At the minimal nitrate concentration (0.25 mmol/L), biosilica content peaked at 49.5 mg/g. With increasing concentrations of nitrate, there was a gradual decrease in biosilica content, which then stabilized within the range of 1.98–3.96 mmol/L. In contrast, the lowest phosphate concentration yielded the minimal biosilica content of 28.9 mg/g, approximately 40% lower than the maximal content of 48.3 mg/g observed at a phosphate concentration of 114.8 μmol/L. However, an increase in phosphate concentration from 114.8 to 229.6 μmol/L led to a significant reduction in biosilica content, contrary to expectations of an increase.

Table 4 Valve diameter and biosilica content of *C. cryptica* under different phosphate levels

Concentration		Valve diameter (μm)	Biosilica content (mg/g)
Nitrate (mmol/L)	0.25	6.4±0.7^{b}	49.5±3.3^{a}
	0.49	6.7±1.0^{b}	46.9±5.7^{a}
	0.99	10.1±1.9^{a}	42.1±4.9^{ab}
	1.98	11.2±2.1^{a}	34.9±3.1^{b}
	3.96	6.2±0.6^{b}	36.3±5.6^{b}
Phosphate (μmol/L)	14.4	6.2±1.0^{c}	28.9±4.7^{c}
	28.7	7.5±1.3^{b}	33.9±3.1^{c}
	57.4	10.1±1.9^{a}	42.1±4.9^{ab}
	114.8	9.3±1.6^{a}	48.3±2.1^{a}
	229.6	6.3±1.0^{c}	41.1±1.8^{b}

Values are shown as mean±SD (n=3). For valve diameter, n=10–19; for biosilica content, n=3. Different letters of superscripts in the same column indicate statistically significant difference between groups (P<0.05).

3.5 Impact of nitrate and phosphate on the transcriptional regulation of silicalemma transmembrane proteins

The transcriptional responses of five genes to varying concentrations of nitrate displayed a pattern similar to that observed with phosphate. As depicted in Fig.5a & b, the transcription levels of *CcSin1* and *CcSin2* decreased significantly on Days 4 and 8 as nitrate concentrations increased from 0.25 to 0.99 mmol/L, and then stabilized within the range of 0.99–3.96 mmol/L. On Day 12, the transcriptional levels of these two genes initially increased with rising nitrate levels, peaking at 0.49 mmol/L, before declining to stabilize within the range of 0.99–3.96 mmol/L. Regarding *CcSAP1*, its transcription levels remained stable on Days 4 and 12, but displayed a downward trend with increased nitrate concentrations on Day 8 (Fig.5c). *CcSAP2* and *CcSAP3* exhibited similar patterns, decreasing with increased nitrate concentrations at almost all three time points, although the variations in *CcSAP2* were less pronounced than those in *CcSAP3* (Fig.5d & e). The phosphate-induced regulatory patterns mirrored those observed with nitrate. At all three time points, transcription levels of *CcSin1* and *CcSin2* decreased with rising phosphate concentrations (Fig.5f & g). The transcriptional levels of *CcSAP1* remained stable in all phosphate treatments throughout the entire cultivation period (Fig.5h). Additionally, both *CcSAP2* and *CcSAP3* responded negatively to increasing phosphate concentrations, especially on Days 4 and 8 (Fig.5i & j).

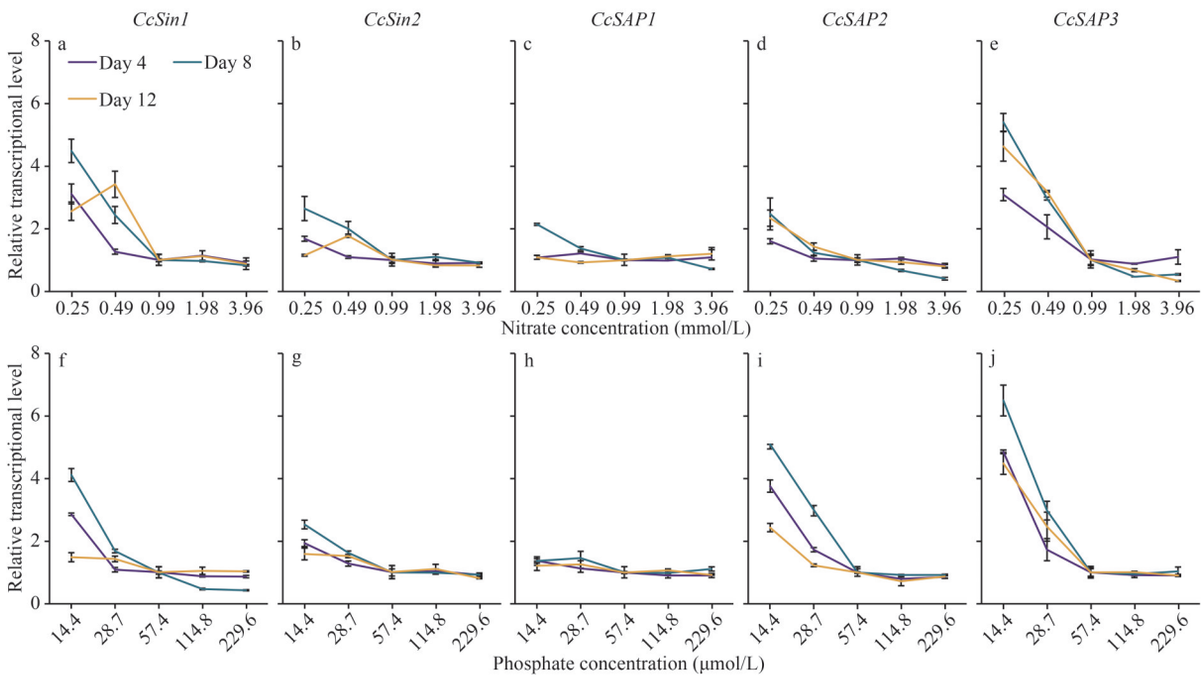

Fig.5 Transcriptional abundances of genes associated with frustule biogenesis under different nitrate (a–e) and phosphate (f–j) levels

Values are presented as mean±SD (n=3); the groups at 0.99-mmol/L nitrate and 57.4-μmol/L phosphate serve as the control groups for the nitrate and phosphate treatments, respectively.

4 DISCUSSION

To provide detailed information for the optimization of cultivation strategy of *C. cryptica* by regulating the nutrients availability, the growth performance, photosynthetic activity, and a series of value-added substances of *C. cryptica* under different nitrate and phosphate concentrations were investigated comprehensively.

4.1 Growth performance and photosynthetic activity

Recent research has substantiated that increasing nutrient levels up to a certain threshold significantly enhances the specific growth rate and biomass accumulation of microalgae, while concentrations exceeding these optimal levels induce physiological stress and inhibit further growth. Assobhi et al. (2024) reported that nitrogen levels up to 17.6-mmol/L $NaNO_3$ optimize chlorophyll synthesis and overall growth of *Chlorococcum* sp. and *Chlamydomonas debaryana*, while increasing nitrogen concentration to 31.76 mmol/L resulted in a marked decline in these parameters, signaling the upper limit of beneficial nutrient addition. The authors also identified 230-μmol/L K_2HPO_4 as the optimal concentration, beyond which no additional growth benefits were observed, suggesting a threshold beyond which further supplementation becomes counterproductive. Corroborating these findings, investigations into *Phaeodactylum tricornutum* revealed similar trends. Afonso et al. (2022) found that gradual increases in nitrate concentration, up to 1.5 g/L, significantly enhanced both growth and fucoxanthin production. However, beyond this level, nutrient utilization efficiency declined, and critical physiological processes began to show signs of disruption. In this study, *C. cryptica* demonstrated significantly diminished growth performance when subjected to 1/4 and 1/2× NMB3# concentrations of either nitrate or phosphate, in comparison to higher nutrient concentrations. This reduction in growth suggests that nitrate levels between 0.25 and 0.49 mmol/L and phosphate levels between 14.4 and 28.7 μmol/L were inadequate to sustain optimal microalgal proliferation. These findings align with previous studies (Afonso et al., 2022; Tavares et al., 2023; Assobhi et al., 2024), which have also reported reduced growth under low nitrogen and phosphorus conditions. However, throughout the examined range, incremental increases in concentrations of nitrate or phosphate consistently improved growth performance, with no inhibitory effects noted at the highest concentrations tested. This phenomenon may be attributed to the fact that the maximum

nitrate and phosphate concentrations used in our experiment were not high enough to reach levels that would inhibit the growth of *C. cryptica*. Nevertheless, an evident deceleration in the growth enhancement rate was observed as nitrate levels increased from 1.98 to 3.96 mmol/L, a trend similarly mirrored in phosphate treatments, suggesting a plateau in growth benefits at these higher nutrient levels.

The above speculations based on growth performance are further supported by assessments of photosynthetic activity. Previous studies have established a robust association between nutrient availability and the photosynthetic efficiency parameter F_v/F_m (Zhao et al., 2017; Carstensen et al., 2018). Typically, microalgae display lower F_v/F_m values under nutrient-deficient conditions, which gradually normalize upon transition to a nutrient-rich medium (Young and Beardall, 2003; Tan et al., 2019). In this study, treatments with 1/4 and 1/2× NMB3# concentrations of nitrate or phosphate consistently displayed significantly lower F_v/F_m values throughout the cultivation period, compared to treatments with higher nutrient concentrations. Moreover, further increases in nitrate from 1.98 to 3.96 mmol/L or in phosphate from 114.8 to 229.6 μmol/L did not lead to appreciable enhancements in F_v/F_m values, as compared to those observed at 0.99-mmol/L nitrate or 57.4-μmol/L phosphate. These results imply the existence of other growth-limiting factors, potentially linked to nutrient imbalances, such as phosphate deficiency at high nitrate levels (1.98 and 3.96 mmol/L) and nitrate deficiency at high phosphate levels (114.8–229.6 μmol/L). Actually, research has shown that nitrogen and phosphorus concentrations, along with their relative N/P ratio, are all crucial in influencing microalgal growth and metabolic efficacy. For instance, optimal N/P ratios significantly enhance growth rates in *Chlorella vulgaris*, while suboptimal ratios reduce photosynthetic efficiency and productivity (Yang et al., 2011; Qian et al., 2024). Potassium nitrate has proven especially effective at an N/P ratio of 16∶1 for boosting *Chlorella vulgaris* growth, and the highest metabolic activity in *Scenedesmus obliquus* was recorded at an N/P ratio of 18∶1 during wastewater treatment (Wu et al., 2014; Gao et al., 2023). In our next steps, we will further investigate the specific impacts of varying N/P ratios to optimize these conditions for enhanced microalgal productivity.

4.2 Macronutrients profile

Generally, lipid accumulation increases under nitrogen starvation across a spectrum of microalgae, including eukaryotic species such as *Tetradesmus obliquus*, *Chlorella vulgaris*, *Mychonastes homosphaera* (Sonkar and Mallick, 2017), *Isochrysis galbana* (Li et al., 2015), and the prokaryotic species *Microcystis* (Cordeiro et al., 2017). Similarly, in *C. cryptica*, cultivation under low nitrate concentrations of 0.25 and 0.49 mmol/L resulted in lipid levels constituting approximately 30% of DCW, significantly higher than other treatments. Furthermore, it is important that while the nitrate concentration of 0.25 mmol/L resulted in the highest lipid content, the lipid productivity was relatively low because the biomass concentration at this nitrate level was only about 30% of that achieved with higher nitrate concentrations ranging from 0.99 to 3.96 mmol/L. In addition to nitrogen, phosphorus limitation is also a critical factor influencing lipid synthesis in microalgae, although the response varies significantly across species. Deficient phosphorus levels have been shown to increase lipid production in *Phaeodactylum tricornutum*, *Chaetoceros* sp., and *Pavlova lutheri*, while causing a reduction in *Nannochloris atomus* and *Tetraselmis* sp. (Reitan et al., 1994; Liang et al., 2013). In the present study, *C. cryptica* exhibited higher lipid concentrations at lower phosphate concentrations (14.4 and 28.7 μmol/L) compared to higher concentrations (57.4–229.6 μmol/L), though the magnitude of differences was less pronounced compared to variations observed under different nitrate conditions. Additionally, *C. cryptica* is recognized for its rich lipid content (Roessler, 1988; Traller et al., 2016). However, our findings indicate that protein levels surpassed lipid contents in four (28.7–229.6 μmol/L) of five phosphate treatments and in three (0.99–3.96 mmol/L) of the five nitrate treatments. This apparent anomaly can be attributed to the cellular phase (early stationary phase) during analysis; it is well established that many microalgae intensify lipid accumulation in the late stationary phase, particularly under conditions of nutrient scarcity.

Contrary to lipids, increased concentrations of nitrate were correlated with higher protein levels in this research, and phosphate showed a similar trend. The extracellular availability of nitrogen and phosphate notably promotes the synthesis of proteins and pigments, which leads to the enhanced

accumulation of primary metabolites such as coenzymes and vitamins in the cells (Zhu et al., 2014; Zhang et al., 2019). Therefore, with sufficient nutrients, cells are likely to achieve peak growth and photosynthetic performance. Conversely, in nutrient-scarce environments, microalgal cells may adjust their metabolic routes, prioritizing the synthesis of lipids and/or carbohydrates, which are essential for energy storage in the cell (Ran et al., 2019).

Carbohydrates are critical for both the structural integrity of the microalgal cell wall and as intracellular energy stores in certain microalgal species. Notably, classes such as Heterokontophyta and Bacillariophyceae tend to favor lipid accumulation over carbohydrates as their primary energy reserves (Al-Jabri et al., 2021; Debnath et al., 2021). Consistent with these findings, *C. cryptica* in our study showed substantially reduced carbohydrate concentrations relative to lipids. Furthermore, our data indicated a progressive reduction in carbohydrate levels as nitrate concentrations increased, while higher levels of phosphate prompted a rise in carbohydrate accumulation. Similar trends have been documented in other representative diatoms, like *Phaeodactylum tricornutum* and *Thalassiosira pseudonana* (Yang et al., 2014; Cruz de Carvalho et al., 2016; Huang et al., 2019), illustrating the diverse effects of nitrogen and phosphorus on carbon management and cellular energy balance in diatoms.

4.3 FA profile

Recent studies have increasingly focused on the utilization of microalgae as natural sources for FAs production, particularly for omega-3 FAs such as EPA and DHA. Cupo et al. (2021) analyzed the FAs composition in both autotrophic and heterotrophic cultures of *C. cryptica*, finding that EPA, along with PA and POA, consistently dominated the FAs profile across different trophic modes. Pahl et al. (2010) also demonstrated that *C. cryptica* is rich in PA, POA, and EPA. Our results generally align with these findings, with exceptions noted under conditions of the highest nitrate concentration and the lowest phosphate concentration, where HTA emerged as a dominant FA, accompanied by a notable decrease in EPA levels.

It is typically observed that microalgae under nitrate-deficient conditions exhibit lower growth rates and tend to accumulate higher levels of SFAs. Conversely, conditions that promote higher growth rates favor the accumulation of PUFAs (Yaakob et al., 2021). For example, Anto et al. (2019) reported that nitrate deprivation induced a sharp decrease in growth rate, along with a significant increase in SFAs and MUFAs, but a decrease in PUFAs in *Chlorella* sp. Being consistent with this pattern, our studies indicate that in treatments with low nitrate concentrations, SFAs including PA and SA were substantially elevated compared to other conditions, while PUFAs such as HDDA and HTA showed a contrary variation pattern. Intriguingly, increases in nitrate concentration from 0.99 to 3.96 mmol/L led to decreases, rather than increases, in EPA levels, underscoring the complex relationship between nitrate availability and EPA accumulation.

Our data also revealed that increased phosphate concentrations significantly decreased MUFA levels in favor of PUFAs, while SFA levels remained relatively stable. This response pattern mirrors the differences observed between autotrophic and heterotrophic *C. cryptica* (Cupo et al., 2021). Similarly, Qari and Oves (2020) reported in *Chlamydomonas reinhardtii* that decreased phosphorus levels led to an increase in SFAs and MUFAs, accompanied by a decline in PUFAs, whereas higher phosphorus concentrations resulted in the opposite trend. A comparable pattern was also observed in the *Monodus subterraneus* by Khozin-Goldberg and Cohen (2006). The underlying mechanisms of these observations warrant further investigation to fully understand the implications. Additionally, it has been reported that FAs profile characterized by high MUFAs, low PUFAs, and optimal SFAs is preferable for biodiesel production (Manzoor et al., 2022). Our findings suggest that adjusting phosphate concentrations could be an effective strategy for optimizing the FAs profile in *C. cryptica* to enhance the biodiesel quality from this microalga.

4.4 Carotenoid

Fucoxanthin shows a wide variety of bioactive properties, including anti-obesity, anti-cancer, anti-inflammatory effects (Kim and Pangestuti, 2011; Fernandes and Mamatha, 2023). Previously, the production of fucoxanthin was mainly based on seaweeds, while recent studies found that the fucoxanthin content in microalgae is 1 or even 2 orders of magnitude higher than that of the macroalgae. Therefore, the interest of producing fucoxanthin based on microalgae is increasing (Seth et al., 2021). Guo et al. (2016) tested the growth and

fucoxanthin content of 13 diatoms species, finding that *C. cryptica* with a fucoxanthin content around 1% of DCW is one of the best sources for fucoxanthin production.

Fucoxanthin content in microalgae varies with nutrient availability. Chen et al. (2024) reported that fucoxanthin content in *Pavlova* sp. peaked at 36.47 mg/g with 400-mg/L $NaNO_3$, compared to 33.13 mg/g at 200 mg/L and 34.76 mg/g at 800 mg/L. Yoshida et al. (2023) examined the effect of $NaNO_3$ concentrations on *P. gyrans*, finding maximum fucoxanthin levels of 4.2, 6.6, and 6.4 mg/g on Days 1, 2, and 3 with 2.4-, 4.8-, and 9.6-mmol/L $NaNO_3$, respectively. These observations align with our findings. Moreover, the phenomenon that fucoxanthin increases with nitrate concentrations also explains the enhanced biomass content, specific growth rate, and F_v/F_m observed from the treatments with higher nitrate concentrations. Unlike the effects of nitrate, the influence of varying phosphate concentrations on fucoxanthin production in *C. cryptica* remains undocumented. Nonetheless, research involving other species, such as *Isochrysis* sp. and *Thalassiosira weissflogii*, indicates that while phosphate enrichment can increase fucoxanthin levels, its impact is notably less pronounced compared to nitrate (Sun et al., 2019; Marella and Tiwari, 2020).

Unlike fucoxanthin, diadinoxanthin participates in a unique and efficient xanthophyll cycle, known as the diadinoxanthin cycle, alongside its epoxy-free counterpart, diatoxanthin, which plays a crucial role in protecting against photoinhibition (Kuczynska et al., 2020). A study by Yoshida et al. (2023) reported that diadinoxanthin levels are significantly influenced by nitrogen concentration, with higher nitrogen levels prompting its accumulation. This reduction under nitrogen depletion is likely linked to the role of diadinoxanthin as a precursor in the fucoxanthin biosynthesis pathway (Cao et al., 2023). Research related to the effect of phosphorus on diadinoxanthin is limited. In this study, our findings show that the variation patterns of diadinoxanthin in response to nitrate and phosphate are similar to those observed for fucoxanthin.

4.5 Frustule biogenesis

The silicified frustule is a hallmark of diatoms and serves as a valuable source for biomaterials production (Wang et al., 2023; Yang et al., 2023). Like all biological materials, the morphology and physicochemical properties of frustules are shaped by environmental conditions such as salinity, temperature, and pH (Su et al., 2018; Wang et al., 2023). For example, Roubeix and Lancelot (2008) observed significant decreases in cell width and height of *Cyclotella meneghiniana* with increasing salinity. Similar patterns were also recorded in *Thalassiosira pseudonana*, where cell height decreased and cell width remained constant under elevated salinity (Hildebrand et al., 2006). Given that the morphological and physicochemical attributes critically influence the performance of frustules when used as biomaterials, understanding how cultivation conditions affects frustule phenotypes is crucial for consistent application efficacy.

In this study, we demonstrate that variations in nitrate and phosphate concentrations significantly affect the valve diameter and biosilica content of frustules in *C. cryptica*. The valve diameter exhibits a distinct bell-shaped response to increasing concentrations of these nutrients. The valve diameter is vital as it determines the specific surface area, which in turn influences nutrient uptake efficiency. However, the link between valve diameter and nutrient uptake efficiency does not fully explain the observed patterns, indicating that further research is needed to elucidate this relationship.

Regarding biosilica content, it drops with increased nitrate but rises with increased phosphate concentrations. Prior studies have linked reduced growth rates, due to nutrient limitation or sub-optimal light conditions, with a higher proportion of cells in the G2+M phase, facilitating increased silicate assimilation for frustule construction (Flynn and Martin-Jézéquel, 2000; Claquin et al., 2002). According to this theory, a decrease in nitrate concentration slows the growth rate and hinder photosynthesis in *C. cryptica*, possibly leading to increased biosilica content. However, this theory does not account for the patterns of biosilica content related to phosphate concentrations observed in this study.

To probe deeper into the complex dynamics of biosilica content, qRT-PCR was employed to assess the transcriptional levels of genes involved in frustule biogenesis under varying nutrient concentrations. Although the role of silaffins in biosilica deposition has been well established (Poulsen and Kröger, 2004; Hildebrand et al., 2018), identifying them in *C. cryptica* is a challenging task due to the absence of conserved amino acid

sequences among diatoms. Hence, we investigated five silicalemma transmembrane proteins, some of which (or their homologs in *Thalassiosira pseudonana*) have been functionally identified previously (Kotzsch et al., 2017; Tesson et al., 2017; Wang et al., 2023).

Unexpectedly, all tested genes were down-regulated with increased nutrient concentrations, responding similarly to changes in both nitrate and phosphate. This observation confirms that increased nitrate levels lead to a reduction in biosilica content. However, it also highlights the complexity of understanding how phosphate levels influence this process. Given that proteins related to biosilica deposition are often highly phosphorylated, it is plausible that phosphate deficiency could impair the activity of kinases essential for phosphorylating these proteins, thereby reducing biosilica content despite the upregulation of biosilica-related gene transcription. Further investigations are necessary to substantiate this hypothesis.

5 CONCLUSION

Nitrate concentrations between 0.25 and 0.49 mmol/L and phosphate concentrations between 14.4 and 28.7 μmol/L were found to be suboptimal for sustaining robust growth of *C. cryptica*, and higher concentrations (0.99–3.96-mmol/L nitrate and 57.4–229.8-μmol/L phosphate) led to improved growth metrics without evident signs of physiological stress.

Elevated nitrate levels increased protein content while decreasing lipid and carbohydrate levels. Conversely, higher phosphate concentrations were associated with increased carbohydrate content and reduced lipid levels, with protein content initially rising and then stabilizing. The FAs composition of *C. cryptica* also showed notable shifts in response to varying nitrate and phosphate levels. Higher nitrate concentrations were correlated with increased levels of PUFAs and decreased SFAs, while higher phosphate levels led to an increase in PUFAs and a decrease in MUFAs. Carotenoid content, including fucoxanthin and diadinoxanthin, increased significantly with elevated nutrient concentrations, indicating that nutrient availability plays a crucial role in the synthesis of these valuable compounds. Additionally, the frustule morphology and biosilica content of *C. cryptica* were significantly influenced by nitrate and phosphate concentrations. Frustules exhibited morphological abnormalities at the lowest and highest nutrient concentrations, indicating that extreme nutrient conditions can adversely affect frustule integrity. A bell-shaped response was observed for valve diameter with varying nutrient levels. Unexpectedly, biosilica content decreased with increasing nitrate levels but increased with rising phosphate levels. Combined with the qRT-PCR results, it can be speculated that a decrease in nitrate concentration results in an increased proportion of cells in the G2+M phase, thereby leading to increased biosilica content. However, the phosphate limitation may weaken the activity of kinases responsible for phosphorylating the frustule biogenesis proteins, thereby ultimately reducing biosilica content.

6 DATA AVAILABILITY STATEMENT

The datasets generated and/or analyzed during the current study are available from the corresponding author on reasonable request.

References

Afonso C, Bragança A R, Rebelo B A et al. 2022. Optimal nitrate supplementation in *Phaeodactylum tricornutum* culture medium increases biomass and fucoxanthin production. *Foods*, **11**(4): 568, http://doi.org/10.3390/foods11040568.

Alipanah L, Winge P, Rohloff J et al. 2018. Molecular adaptations to phosphorus deprivation and comparison with nitrogen deprivation responses in the diatom *Phaeodactylum tricornutum*. *PLoS One*, **13**(2): e0193335, http://doi.org/10.1371/journal.pone.0193335.

Al-Jabri H, Das P, Khan S et al. 2021. Treatment of wastewaters by microalgae and the potential applications of the produced biomass-a review. *Water*, **13**(1): 27, http://doi.org/10.3390/w13010027.

Anto S, Pugazhendhi A, Mathimani T. 2019. Lipid enhancement through nutrient starvation in *Chlorella* sp. and its fatty acid profiling for appropriate bioenergy feedstock. *Biocatalysis and Agricultural Biotechnology*, **20**: 101179, http://doi.org/10.1016/j.bcab.2019.101179.

Assobhi B, Ennasry H, Latique S et al. 2024. Influence of salinity, nitrogen and phosphorus concentrations on the physiological and biochemical characteristics of two Chlorophyceae isolated from Fez freshwater, Morocco. *Scientific Reports*, **14**(1): 8259, http://doi.org/10.1038/s41598-024-58864-4.

Bligh E G, Dyer W J. 1959. A rapid method of total lipid extraction and purification. *Canadian Journal of Biochemistry and Physiology*, **37**(8): 911-917, http://doi.org/10.1139/o59-099.

Brembu T, Mühlroth A, Alipanah L et al. 2017. The effects of phosphorus limitation on carbon metabolism in diatoms. *Philosophical Transactions of the Royal Society B*:

Biological Sciences, **372**(1728): 20160406, http://doi.org/10.1098/rstb.2016.0406.

Cañavate J P, Armada I, Hachero-Cruzado I. 2017. Aspects of phosphorus physiology associated with phosphate-induced polar lipid remodelling in marine microalgae. *Journal of Plant Physiology*, **214**: 28-38, http://doi.org/10.1016/j.jplph.2017.03.019.

Cao T J, Bai Y, Buschbeck P et al. 2023. An unexpected hydratase synthesizes the green light-absorbing pigment fucoxanthin. *The Plant Cell*, **35**(8): 3053-3072, http://doi.org/10.1093/plcell/koad116.

Carstensen A, Herdean A, Schmidt S B et al. 2018. The impacts of phosphorus deficiency on the photosynthetic electron transport chain. *Plant Physiology*, **177**(1): 271-284, http://doi.org/10.1104/pp.17.01624.

Chauton M S, Olsen Y, Vadstein O. 2013. Biomass production from the microalga *Phaeodactylum tricornutum*: nutrient stress and chemical composition in exponential fed-batch cultures. *Biomass & Bioenergy*, **58**: 87-94, http://doi.org/10.1016/j.biombioe.2013.10.004.

Chen C Y, Liu P Y, Chang Y H et al. 2024. Optimizing cultivation strategies and scaling up for fucoxanthin production using *Pavlova* sp. *Bioresource Technology*, **399**: 130609, http://doi.org/10.1016/j.biortech.2024.130609.

Chiriboga O, Rorrer G L. 2018. Effects of nitrogen delivery on chitin nanofiber production during batch cultivation of the diatom *Cyclotella* sp. in a bubble column photobioreactor. *Journal of Applied Phycology*, **30**(3): 1575-1581, http://doi.org/10.1007/s10811-017-1368-z.

Chiriboga O, Rorrer G L. 2019. Phosphate addition strategies for enhancing the co-production of lipid and chitin nanofibers during fed-batch cultivation of the diatom *Cyclotella* sp. *Algal Research*, **38**: 101403, http://doi.org/10.1016/j.algal.2018.101403.

Claquin P, Martin-Jézéquel V, Kromkamp J C et al. 2002. Uncoupling of silicon compared with carbon and nitrogen metabolisms and the role of the cell cycle in continuous cultures of *Thalassiosira pseudonana* (Bacillariophyceae) under light, nitrogen, and phosphorus control. *Journal of Phycology*, **38**(5): 922-930, http://doi.org/10.1046/j.1529-8817.2002.t01-1-01220.x.

Cooney M J, Young G, Pate R. 2011. Bio-oil from photosynthetic microalgae: case study. *Bioresource Technology*, **102**(1): 166-177, http://doi.org/10.1016/j.biortech.2010.06.134.

Cordeiro R S, Vaz I C D, Magalhães S M S et al. 2017. Effects of nutritional conditions on lipid production by cyanobacteria. *Anais da Academia Brasileira de Ciências*, **89**(3S): 2021-2031, http://doi.org/10.1590/0001-3765201720150707.

Cruz de Carvalho M H, Sun H X, Bowler C et al. 2016. Noncoding and coding transcriptome responses of a marine diatom to phosphate fluctuations. *New Phytologist*, **210**(2): 497-510, http://doi.org/10.1111/nph.13787.

Cupo A, Landi S, Morra S et al. 2021. Autotrophic vs. heterotrophic cultivation of the marine diatom *Cyclotella cryptica* for EPA production. *Marine Drugs*, **19**(7): 355, http://doi.org/10.3390/md19070355.

Debnath C, Bandyopadhyay T K, Bhunia B et al. 2021. Microalgae: sustainable resource of carbohydrates in third-generation biofuel production. *Renewable & Sustainable Energy Reviews*, **150**: 111464, http://doi.org/10.1016/j.rser.2021.111464.

Dunahay T G, Jarvis E E, Roessler P G. 1995. Genetic transformation of the diatoms *Cyclotella cryptica* and *Navicula saprophila*. *Journal of Phycology*, **31**(6): 1004-1012, http://doi.org/10.1111/j.0022-3646.1995.01004.x.

Fang J Q, Sun Y, Zhu Z J et al. 2024. Algae-bacteria consortia promotes the cell growth of marine microalgae *Phaeodactylum tricornutum* and *Chrysotila roscoffensis*. *Algal Research*, **80**: 103535, http://doi.org/10.1016/j.algal.2024.103535.

Feng T Y, Yang Z K, Zheng J W et al. 2015. Examination of metabolic responses to phosphorus limitation via proteomic analyses in the marine diatom *Phaeodactylum tricornutum*. *Scientific Reports*, **5**: 10373, http://doi.org/10.1038/srep10373.

Fernandes V, Mamatha B S. 2023. Fucoxanthin, a functional food ingredient: challenges in bioavailability. *Current Nutrition Reports*, **12**(4): 567-580, http://doi.org/10.1007/s13668-023-00492-x.

Flynn K J, Martin-Jézéquel V. 2000. Modelling Si-N-limited growth of diatoms. *Journal of Plankton Research*, **22**(3): 447-472, http://doi.org/10.1093/plankt/22.3.447.

Gao L, Ding W Q, Xi J J et al. 2023. Effects of different nitrogen/phosphorus ratios on the growth and metabolism of microalgae *Scenedesmus obliquus* cultured in the mixed wastewater from primary settling tank and sludge thickener. *Process Safety and Environmental Protection*, **170**: 824-833, http://doi.org/10.1016/j.psep.2022.12.059.

Guo B B, Liu B, Yang B et al. 2016. Screening of diatom strains and characterization of *Cyclotella cryptica* as a potential fucoxanthin producer. *Marine Drugs*, **14**(7): 125, http://doi.org/10.3390/md14070125.

Han J C, Thomsen L, Pan K H et al. 2018. Two-step process: enhanced strategy for wastewater treatment using microalgae. *Bioresource Technology*, **268**: 608-615, http://doi.org/10.1016/j.biortech.2018.08.054.

Hildebrand M, Lerch S J L, Shrestha R P. 2018. Understanding diatom cell wall silicification—moving forward. *Frontiers in Marine Science*, **5**: 125, http://doi.org/10.3389/fmars.2018.00125.

Hildebrand M, York E, Kelz J I et al. 2006. Nanoscale control of silica morphology and three-dimensional structure during diatom cell wall formation. *Journal of Materials Research*, **21**(10): 2689-2698, http://doi.org/10.1557/jmr.2006.0333.

Hsieh K M, Lion L W, Shuler M L. 1985. Bioreactor for the study of defined interactions of toxic metals and biofilms. *Applied and Environmental Microbiology*, **50**(5): 1155-1161, http://doi.org/10.1128/aem.50.5.1155-1161.1985.

Huang B, Marchand J, Blanckaert V et al. 2019. Nitrogen

and phosphorus limitations induce carbon partitioning and membrane lipid remodelling in the marine diatom *Phaeodactylum tricornutum*. *European Journal of Phycology*, **54**(3): 342-358, http://doi.org/10.1080/09670262.2019.1567823.

Huesemann M H, Hausmann T S, Bartha R et al. 2009. Biomass productivities in wild type and pigment mutant of *Cyclotella* sp. (Diatom). *Applied Biochemistry and Biotechnology*, **157**(3): 507-526, http://doi.org/10.1007/s12010-008-8298-9.

Khan M I, Shin J H, Kim J D. 2018. The promising future of microalgae: current status, challenges, and optimization of a sustainable and renewable industry for biofuels, feed, and other products. *Microbial Cell Factories*, **17**: 36, http://doi.org/10.1186/s12934-018-0879-x.

Khozin-Goldberg I, Cohen Z. 2006. The effect of phosphate starvation on the lipid and fatty acid composition of the fresh water eustigmatophyte *Monodus subterraneus*. *Phytochemistry*, **67**(7): 696-701, http://doi.org/10.1016/j.phytochem.2006.01.010.

Kim S K, Pangestuti R. 2011. Biological activities and potential health benefits of fucoxanthin derived from marine brown algae. *Advances in Food and Nutrition Research*, **64**: 111-128, http://doi.org/10.1016/B978-0-12-387669-0.00009-0.

Kirkham A R, Richthammer P, Schmidt K et al. 2017. A role for the cell-wall protein silacidin in cell size of the diatom *Thalassiosira pseudonana*. *The ISME Journal*, **11**(11): 2452-2464, http://doi.org/10.1038/ismej.2017.100.

Kotzsch A, Gröger P, Pawolski D et al. 2017. Silicanin-1 is a conserved diatom membrane protein involved in silica biomineralization. *BMC Biology*, **15**: 65, http://doi.org/10.1186/s12915-017-0400-8.

Kuczynska P, Jemiola-Rzeminska M, Nowicka B et al. 2020. The xanthophyll cycle in diatom *Phaeodactylum tricornutum* in response to light stress. *Plant Physiology and Biochemistry*, **152**: 125-137, http://doi.org/10.1016/j.plaphy.2020.04.043.

Kumar K, Mishra S K, Shrivastav A et al. 2015. Recent trends in the mass cultivation of algae in raceway ponds. *Renewable and Sustainable Energy Reviews*, **51**: 875-885, http://doi.org/10.1016/j.rser.2015.06.033.

Laws E A, Taguchi S, Hirata J et al. 1988. Optimization of microalgal production in a shallow outdoor flume. *Biotechnology and Bioengineering*, **32**(2): 140-147, http://doi.org/10.1002/bit.260320204.

Li Y X, Zhao F J, Yu D D. 2015. Effect of nitrogen limitation on cell growth, lipid accumulation and gene expression in *Chlorella sorokiniana*. *Brazilian Archives of Biology and Technology*, **58**(3): 462-467, http://doi.org/10.1590/s1516-8913201500391.

Liang K H, Zhang Q H, Gu M et al. 2013. Effect of phosphorus on lipid accumulation in freshwater microalga *Chlorella* sp. *Journal of Applied Phycology*, **25**(1): 311-318, http://doi.org/10.1007/s10811-012-9865-6.

Liu M S, Hellebust J A. 1974. Utilization of amino acids as nitrogen sources, and their effects on nitrate reductase in the marine diatom *Cyclotella cryptica*. *Canadian Journal of Microbiology*, **20**(8): 1119-1125, http://doi.org/10.1139/m74-174.

Lu X, Zhao W X, Wang J et al. 2024. A comprehensive review on the heterotrophic production of bioactive compounds by microalgae. *World Journal of Microbiology & Biotechnology*, **40**(7): 210, http://doi.org/10.1007/s11274-024-03892-5.

Manzoor M, Hussain A, Ahmad Q U A et al. 2022. Biodiesel quality assessment of microalgae cultivated mixotrophically on sugarcane bagasse. *Sustainable Energy Technologies and Assessments*, **53**: 102359, http://doi.org/10.1016/j.seta.2022.102359.

Marella T K, Tiwari A. 2020. Marine diatom *Thalassiosira weissflogii* based biorefinery for co-production of eicosapentaenoic acid and fucoxanthin. *Bioresource Technology*, **307**: 123245, http://doi.org/10.1016/j.biortech.2020.123245.

Ozkan A, Rorrer G L. 2017a. Effects of light intensity on the selectivity of lipid and chitin nanofiber production during photobioreactor cultivation of the marine diatom *Cyclotella* sp. *Algal Research*, **25**: 216-227, http://doi.org/10.1016/j.algal.2017.04.032.

Ozkan A, Rorrer G L. 2017b. Effects of CO_2 delivery on fatty acid and chitin nanofiber production during photobioreactor cultivation of the marine diatom *Cyclotella* sp. *Algal Research*, **26**: 422-430, http://doi.org/10.1016/j.algal.2017.07.003.

Pahl S L, Lewis D M, Chen F et al. 2010. Growth dynamics and the proximate biochemical composition and fatty acid profile of the heterotrophically grown diatom *Cyclotella cryptica*. *Journal of Applied Phycology*, **22**(2): 165-171, http://doi.org/10.1007/s10811-009-9436-7.

Pahl S L, Lewis D M, King K D et al. 2012. Heterotrophic growth and nutritional aspects of the diatom *Cyclotella cryptica* (Bacillariophyceae): effect of nitrogen source and concentration. *Journal of Applied Phycology*, **24**(2): 301-307, http://doi.org/10.1007/s10811-011-9680-5.

Poulsen N, Kröger N. 2004. Silica morphogenesis by alternative processing of silaffins in the diatom *Thalassiosira pseudonana*. *Journal of Biological Chemistry*, **279**(41): 42993-42999, http://doi.org/10.1074/jbc.M407734200.

Qari H A, Oves M. 2020. Fatty acid synthesis by *Chlamydomonas reinhardtii* in phosphorus limitation. *Journal of Bioenergetics and Biomembranes*, **52**(1): 27-38, http://doi.org/10.1007/s10863-019-09813-8.

Qian W Y, Yang Y N, Chou S et al. 2024. Effect of N/P ratio on attached microalgae growth and the differentiated metabolism along the depth of biofilm. *Environmental Research*, **240**: 117428, http://doi.org/10.1016/j.envres.2023.117428.

Ran W Y, Wang H T, Liu Y H et al. 2019. Storage of starch and lipids in microalgae: biosynthesis and manipulation by nutrients. *Bioresource Technology*, **291**: 121894, http://doi.org/10.1016/j.biortech.2019.121894.

Ras M, Steyer J P, Bernard O. 2013. Temperature effect on

microalgae: a crucial factor for outdoor production. *Reviews in Environmental Science and Bio/Technology*, **12**(2): 153-164, http://doi.org/10.1007/s11157-013-9310-6.

Reitan K I, Rainuzzo J R, Olsen Y. 1994. Effect of nutrient limitation on fatty acid and lipid content of marine microalgae. *Journal of Phycology*, **30**(6): 972-979, http://doi.org/10.1111/j.0022-3646.1994.00972.x.

Roessler P G. 1988. Effects of silicon deficiency on lipid composition and metabolism in the diatom *Cyclotella cryptica*. *Journal of Phycology*, **24**(3): 394-400, http://doi.org/10.1111/j.1529-8817.1988.tb04482.x.

Roubeix V, Lancelot C. 2008. Effect of salinity on growth, cell size and silicification of an euryhaline freshwater diatom: *Cyclotella meneghiniana* Kütz. *Transitional Waters Bulletin*, **2**(1): 31-38, http://doi.org/10.1285/i1825229Xv2n1p31.

Sedmak J J, Grossberg S E. 1977. A rapid, sensitive, and versatile assay for protein using Coomassie Brilliant Blue G250. *Analytical Biochemistry*, **79**(1-2): 544-552, http://doi.org/10.1016/0003-2697(77)90428-6.

Seth K, Kumar A, Rastogi R P et al. 2021. Bioprospecting of fucoxanthin from diatoms-Challenges and perspectives. *Algal Research*, **60**: 102475, http://doi.org/10.1016/j.algal.2021.102475.

Shifrin N S, Chisholm S W. 1981. Phytoplankton lipids: interspecific differences and effects of nitrate, silicate and light-dark cycles. *Journal of Phycology*, **17**(4): 374-384, http://doi.org/https://doi.org/10.1111/j.1529-8817.1981.tb00865.x.

Slocombe S P, Zhang Q Y, Ross M et al. 2015. Unlocking nature's treasure-chest: screening for oleaginous algae. *Scientific Reports*, **5**: 9844, http://doi.org/10.1038/srep09844.

Sonkar S, Mallick N. 2017. Development of a single phase nitrate feeding strategy for enhanced lipid productivity from green microalgae for biodiesel production. *Environmental Progress & Sustainable Energy*, **36**(1): 222-231, http://doi.org/10.1002/ep.12443.

Sriharan S, Bagga D, Nawaz M. 1991. The effects of nutrients and temperature on biomass, growth, lipid production, and fatty acid composition of *Cyclotella cryptica* Reimann, Lewin, and Guillard. *Applied Biochemistry and Biotechnology*, **28**(1): 317-326, http://doi.org/10.1007/BF02922611.

Su Y Y, Lundholm N, Ellegaard M. 2018. The effect of different light regimes on diatom frustule silicon concentration. *Algal Research*, **29**: 36-40, http://doi.org/10.1016/j.algal.2017.11.014.

Sun Y, Xin Y, Zhang L Y et al. 2022. Enhancement of violaxanthin accumulation in *Nannochloropsis oceanica* by overexpressing a carotenoid isomerase gene from *Phaeodactylum tricornutum*. *Frontiers in Microbiology*, **13**: 942883, http://doi.org/10.3389/fmicb.2022.942883.

Sun Z, Wang X F, Liu J. 2019. Screening of *Isochrysis* strains for simultaneous production of docosahexaenoic acid and fucoxanthin. *Algal Research*, **41**: 101545, http://doi.org/10.1016/j.algal.2019.101545.

Tan L J, Xu W J, He X L et al. 2019. The feasibility of F_v/F_m on judging nutrient limitation of marine algae through indoor simulation and *in situ* experiment. *Estuarine, Coastal and Shelf Science*, **229**: 106411, http://doi.org/10.1016/j.ecss.2019.106411.

Tavares L, Nudi M H, Arroyo P A et al. 2023. Effect of different concentrations of phosphorus and nitrogen on the growth of the microalgae *Chlorella vulgaris*. *International Journal of Energy and Environmental Engineering*, **14**(4): 563-572, http://doi.org/10.1007/s40095-022-00535-z.

Tesson B, Lerch S J L, Hildebrand M. 2017. Characterization of a new protein family associated with the silica deposition vesicle membrane enables genetic manipulation of diatom silica. *Scientific Reports*, **7**: 13457, http://doi.org/10.1038/s41598-017-13613-8.

Tilman D, Kilham S S. 1976. Phosphate and silicate growth and uptake kinetics of the diatoms *Asterionella formosa* and *Cyclotella meneghiniana* in batch and semicontinuous culture. *Journal of Phycology*, **12**(4): 375-383, http://doi.org/10.1111/j.1529-8817.1976.tb02860.x.

Traller J C, Cokus S J, Lopez D A et al. 2016. Genome and methylome of the oleaginous diatom *Cyclotella cryptica* reveal genetic flexibility toward a high lipid phenotype. *Biotechnology for Biofuels*, **9**: 258, http://doi.org/10.1186/s13068-016-0670-3.

Wang L L, Sun Y, Zhang R H et al. 2023. Enhancement of hemostatic properties of *Cyclotella cryptica* frustule through genetic manipulation. *Biotechnology for Biofuels and Bioproducts*, **16**(1): 136, http://doi.org/10.1186/s13068-023-02389-x.

Wu J S, Jia R B, Li B et al. 2014. Study on the correlation of N, P nutrients and *Chlorella* growth. *Applied Mechanics and Materials*, **641-642**: 1183-1186, http://doi.org/10.4028/www.scientific.net/AMM.641-642.1183.

Yaakob M A, Mohamed R M S R, Al-Gheethi A et al. 2021. Influence of nitrogen and phosphorus on microalgal growth, biomass, lipid, and fatty acid production: an overview. *Cells*, **10**(2): 393, http://doi.org/10.3390/cells10020393.

Yang C F, Feng C, Li Y H et al. 2023. Morphological and physicochemical characteristics, biological functions, and biomedical applications of diatom frustule. *Algal Research*, **72**: 103104, http://doi.org/10.1016/j.algal.2023.103104.

Yang J, Xu M, Zhang X Z et al. 2011. Life-cycle analysis on biodiesel production from microalgae: water footprint and nutrients balance. *Bioresource Technology*, **102**(1): 159-165, http://doi.org/10.1016/j.biortech.2010.07.017.

Yang Z K, Zheng J W, Niu Y F et al. 2014. Systems-level analysis of the metabolic responses of the diatom *Phaeodactylum tricornutum* to phosphorus stress. *Environmental Microbiology*, **16**(6): 1793-1807, http://doi.org/10.1111/1462-2920.12411.

Yoshida E, Kato Y, Kanamoto A et al. 2023. Metabolomic analysis of the effect of nitrogen on fucoxanthin synthesis by the haptophyte *Pavlova gyrans*. *Algal Research*, **72**: 103144, http://doi.org/10.1016/j.algal.2023.103144.

Young E B, Beardall J. 2003. Photosynthetic function in *Dunaliella tertiolecta* (Chlorophyta) during a nitrogen starvation and recovery cycle. *Journal of Phycology*, **39**(5): 897-905, http://doi.org/10.1046/j.1529-8817.2003.03042.x.

Zhang W H, Wu J, Weng L Y et al. 2020. An improved phenol-sulfuric acid method for the determination of carbohydrates in the presence of persulfate. *Carbohydrate Polymers*, **227**: 115332, http://doi.org/10.1016/j.carbpol.2019.115332.

Zhang Y, Wu H J, Yuan C J et al. 2019. Growth, biochemical composition, and photosynthetic performance of *Scenedesmus acuminatus* during nitrogen starvation and resupply. *Journal of Applied Phycology*, **31**(5): 2797-2809, http://doi.org/10.1007/s10811-019-01783-z.

Zhao L S, Li K, Wang Q M et al. 2017. Nitrogen starvation impacts the photosynthetic performance of *Porphyridium cruentum* as revealed by chlorophyll *a* fluorescence. *Scientific Reports*, **7**: 8542, http://doi.org/10.1038/s41598-017-08428-6.

Zhu B H, Shen H, Li Y et al. 2020. Large-scale cultivation of *Spirulina* for biological CO_2 mitigation in open raceway ponds using purified CO_2 from a coal chemical flue gas. *Frontiers in Bioengineering and Biotechnology*, **7**: 441, http://doi.org/10.3389/fbioe.2019.00441.

Zhu S N, Wang Y J, Huang W et al. 2014. Enhanced accumulation of carbohydrate and starch in *Chlorella zofingiensis* induced by nitrogen starvation. *Applied Biochemistry and Biotechnology*, **174**(7): 2435-2445, http://doi.org/10.1007/s12010-014-1183-9.